Differential phase technique with the Keck Interferometer

Rachel Akeson[a], Mark Swain[b] and Mark Colavita[b]

[a] Infrared Processing and Analysis Center, California Institute of Technology, Pasadena, CA, USA

[b] Jet Propulsion Lab, California Institute of Technology, 4800 Oak Grove Drive, Pasadena, CA, 91109 USA

ABSTRACT

We will present the motivation and development of the novel "differential phase" technique being developed for the Keck Interferometer. The differential phase technique is a form of self phased reference, chromatic astrometry. Using the Keck Interferometer, we intend to make these measurements in the H, K, L, and M bands; atmospheric dispersion compensation and common mode refractive index estimation are necessary to reach the design goal of 0.1 miliradians of inter-band phase difference sensitivity. We report on test observations taken at the Palomar Testbed Interferometer, including atmospheric dispersion measurement and compensation.

By combining the 10 meter Keck telescopes, this technique will enable measurement and characterization of some of the known extra solar planets, such as the companion to 51 Peg. Because of the large intensity difference between the stellar primary and the planetary companion, we use the differential phase technique to convert a problem of intensity dynamic range to one of phase dynamic range. In addition to enabling the direct detection of extra solar planets, this technique is applicable to other science objectives.

Keywords: infrared interferometry, atmospheric dispersion

1. INTRODUCTION

Direct detection of extrasolar planets is challenging due to the high intensity contrast and small angular separation between the planet and the star. For example, the planet/stellar thermal flux ratio of a Jupiter-size planet orbiting 0.05 pc from a solar-type star is $\sim 10^{-8}$ in the optical. In the infrared, this ratio becomes more tractable; the same planet has a flux ratio of $\sim 10^{-4}$ at 2 μm. While the planet alone could be detected at this level, the nearby star makes this detection a problem of intensity dynamic range and spatial resolution. At a distance of 20 pc, the angular separation of this planetary companion is 2.5 milliarcseconds, smaller than the diffraction limit of a single Keck 10-m telescope. Interferometric techniques can provide both the necessary sensitivity and resolution to study extrasolar planets in the infrared.

2. DIFFERENTIAL PHASE TECHNIQUE

The Palomar Testbed Interferometer (PTI) and the Keck Interferometer are direct detection infrared interferometers with active fringe tracking. PTI is described in detail in Ref. 1. The fringe amplitude and phase are measured by stroking the delay line over a distance of one wavelength and counting the photons in each of four bins, designated A, B, C, and D (see Ref. 2 for more details on this technique). Neglecting the bias term, the squared visibility and phase are then given by

$$V^2 = \frac{\pi}{2} \frac{\langle (A-C)^2 + (B-D)^2 \rangle}{\langle A+B+C+D \rangle^2}$$

$$\phi = \tan^{-1} \frac{B-D}{A-C}.$$

Further author information: (Send correspondence to RA: email akeson@huey.jpl.nasa.gov)

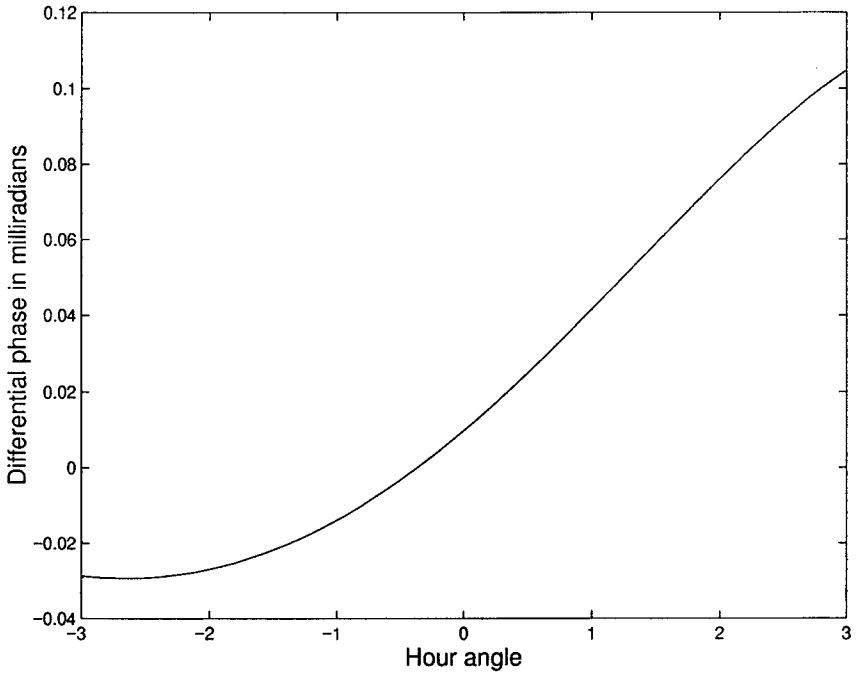

Figure 1. Predicted differential phase between the H and K bands as a function of hour angle for a star and planet binary system like 51 Peg (see section 4.1) as observed by the Keck-Keck baseline.

2.1. Differential phase

In the differential phase mode, the presence of a faint companion is detected by measuring the fringe phase simultaneously at two or more wavelengths. A phase difference as a function of wavelength is produced by sources with different spectral energy distributions, as the source amplitudes will contribute different fractions to the measured fringe at different wavelengths. In the narrow band limit, the fringe from the primary is given by

$$V_p \cos(kx)$$

where k is $2\pi/\lambda$ and x is the delay. The secondary source fringe is given by

$$V_s \cos[k(x+\delta)],$$

where δ is the separation of the two sources on the sky as measured in delay space and is a function of the baseline and ds, the separation on the sky, $\delta = \vec{ds} \cdot \vec{B}$. Both the amplitudes of the fringes V_p and V_s, as well as k will depend on the wavelength band. The relative contribution of the primary and secondary to the photon count for a particular measurement bin, A, B, C, D, is given by

$$A_{\lambda_1} = \int_0^{\lambda_1/4} V_p \cos[k_1 x]\, dx + \int_0^{\lambda_1/4} V_s \cos[k_1 (x+\delta)]\, dx$$

and so on. Once the source flux densities and separation vector are specified, the phase at each wavelength and the differential phase can be easily computed from these integrals. As the interferometer tracks a source across the sky, the projected baseline will evolve in time. Thus, the differential phase for a given source will be a function of hour angle (Figure 1). This evolution of the differential phase can be used to distinguish the true signal from instrumental effects.

As the maximum differential phase effect is approximately the relative source fluxes, it is essential to make very precise phase measurements. One of the two wavelengths will be used as the reference for fringe tracking. The phase

at the second wavelength will be measured simultaneously as an offset phase from the reference wavelength. By using the same beam path for the 2 wavelengths and measuring the phases simultaneously, many systematic effects will be removed from the observed differential phase.

One complication for these multi-wavelength observations is the wavelength dependence of the atmospheric dispersion. If this effect is not corrected, the fringe packets at the two wavelengths will not be at the same location in delay space. An atmospheric dispersion compensator (ADC) is necessary to equalize the phase delay at the two wavelengths.

3. DIFFERENTIAL PHASE AT PTI

3.1. Demonstration observations

As part of the development effort for differential phase, test observations were taken at PTI. A binary target source was specifically chosen to give a large differential phase signature, which is produced by a large color difference between the components and a binary separation of at least a fringe spacing. Given the PTI magnitude and sky coverage limitations, the best differential phase test source was determined to be the spectroscopic binary Iota Peg (HD 210027). During the 1997 and 1998 observing seasons, Iota Peg was observed and its orbital parameters were derived as part of the binary orbit program at PTI.[3]

A differential phase metric can be constructed from any two channel phases. Widely separated wavelengths tend to have larger differential phase values, although this depends on the details of the source spectra. For the PTI data, we have used the group delay as a differential phase metric and concentrated on observations within the K band. As part of the normal observing procedure, the real time system at PTI calculates a group delay estimator every 0.5 seconds. This estimator uses a complex Fourier transform of the channel phases and is analogous to a straight line fit to the channel phases. We use this group delay estimator as a proxy for differential phase as the PTI software was already designed to output this quantity on 0.5 second time scales. The fringe tracker uses the group delay to keep the fringe centered around zero phase delay. If the measurement has sufficient signal-to-noise, a group delay value outside the range $\pm\lambda/2$ will cause the fringe tracker to hop one fringe. Due to compensation of the vacuum delay with a dispersive air path, the fringe and the envelope have slightly different velocities, which correspond to a group delay change of one fringe (2.2 microns) for every $\sim$4 meters of delay. We will refer to this as the sidereal signature.

An example of group delay data showing a clear sidereal signature is given in Figure 2. The data in the top panel are from night 99186 which had low group delay noise, while the bottom panel is data on the same source from night 99169 where the group delay is more noisy. As discussed in section 3.2, our current understanding of the infrared dispersion due to water suggests that the group delay noise is dominated by water vapor fluctuations in the atmosphere, the magnitude of which vary greatly from night to night at PTI.

Before a source can be evaluated for a differential phase signature, the sidereal signature must be measured and removed. The group delay signature is a function of delay and has two parameters, a slope of group delay over delay and an offset in delay. Once this signature and any instrumental effects are removed, any group delay value significantly different from 0 should be due to source characteristics.

Iota Peg was observed for over 2 hours in good weather conditions on night 99304. On this night, only 1 calibrator, HD 209761, was observed. The sidereal signature measured on the calibrator using the above procedure, which produced a best fit slope of -5.85×10^{-7} μm/μm and offset of -2.2×10^{6} μm. The residual rms after removing this sidereal signature is 0.42 μm but the residual time series shows remaining structure within each 130 scan, consistent with water vapor fluctuations, and some low frequency structure over the 2 hour time interval. This low frequency time domain structure was removed by averaging the data points within each scan and interpolating in time. This structure may be caused by instrumental effects or by long term changes in the water column. The sidereal slope and the scan average were both subtracted from the source group delay (Figure 3). The source group delay is clearly offset from zero and is consistent with the predicted differential phase.

The differential phase for Iota Peg is predicted as described in section 2.1 using the orbital parameters from Ref. 3 and the PTI baseline. Blackbody spectra are used for both of the components with spectral types of F5V for the primary and G8V for the secondary, with effective temperatures of 6440 and 5570 K respectively. The flux of the secondary is scaled to match the measured ratio in the K band. The distance to the system is 11.5 parsec.

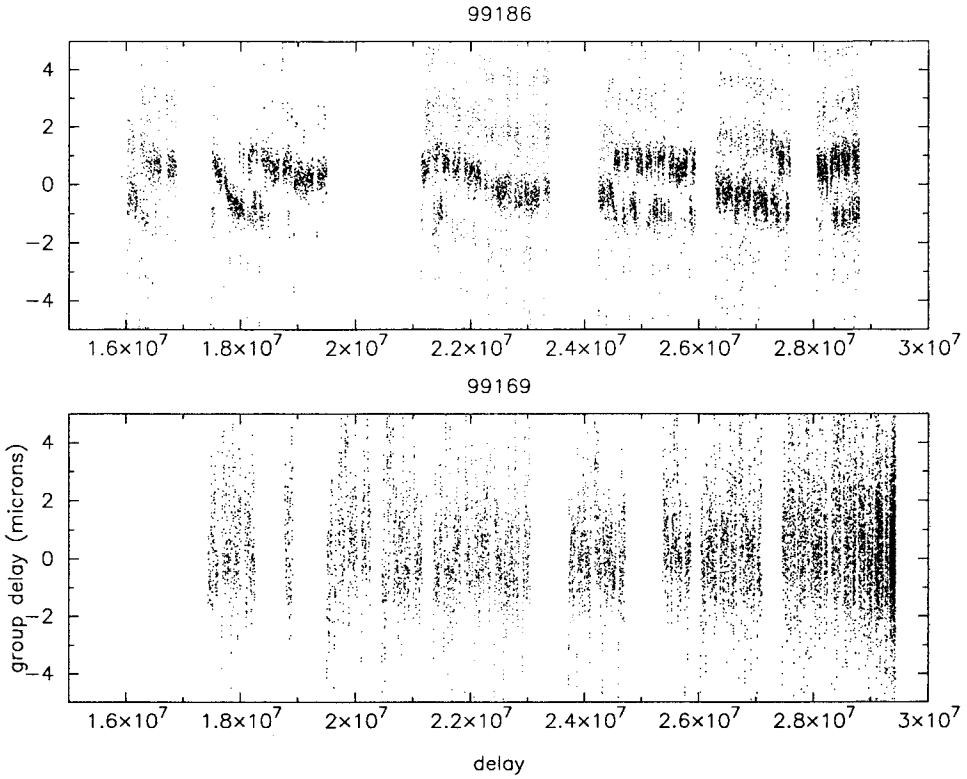

Figure 2. Measured group delay as a function of total delay for two nights at PTI. The top panel (night 99186) shows a night with low group delay noise where the sidereal signature is apparent. The bottom panel (night 99169) shows observations of the same sources on a second night where the group delay noise is much higher. Each point represents 0.5 seconds of data.

3.2. Atmospheric limitations

Motivated by our results from PTI, we considered the possibility that the measured fluctuations in the group delay were due to water vapor fluctuations. Originally we extrapolated the optical phase and group refractivity formula of Ref. 4 to the near-infrared to predict the effects of water and temperature fluctuations on the measurements. These calculations predicted that the dispersion effects of water fluctuations should be lower than those due to temperature fluctuations. However, a more recent work by Ref. 5 derived an expression for the phase refractivity from 10 microns into the far-infrared and at discrete points in the L band (3.5 microns). Comparing the dispersion extrapolated from the optical and infrared results suggests that the optical formula underestimates the dispersion due to water vapor in the near-infrared by a factor of 20. Measurements of the water dispersion in the K band were made at PTI. These results and further calculations by the group which did the original infrared work (Ref. 5) demonstrated that dispersion in the near-infrared is dominated by water vapor fluctuations for the weather conditions typical at PTI and Keck.

We have investigated several techniques to mitigate the effects of water vapor fluctuations. The most straightforward is to use a nearby (separation less than a few arcmin) calibrator source, which is assumed to have no intrinsic differential phase signature, to measure the group delay fluctuations and apply this correction to the source. This method is the most direct; however, not all of the target sources have appropriate calibrators. The water vapor fluctuations can also be estimated using the intensity fluctuations in the water line between the H and K bands. For the total water columns typical for good night at Mauna Kea, this line is not saturated and small changes in the total column result in small changes in the transmission. For these bright target sources ($K_{mag} \sim 5$), this method yields a factor of 10 improvement. A different approach is to take measurements at several different wavelengths and to use the different wavelength dependences of the water vapor and the source differential phase to separate the

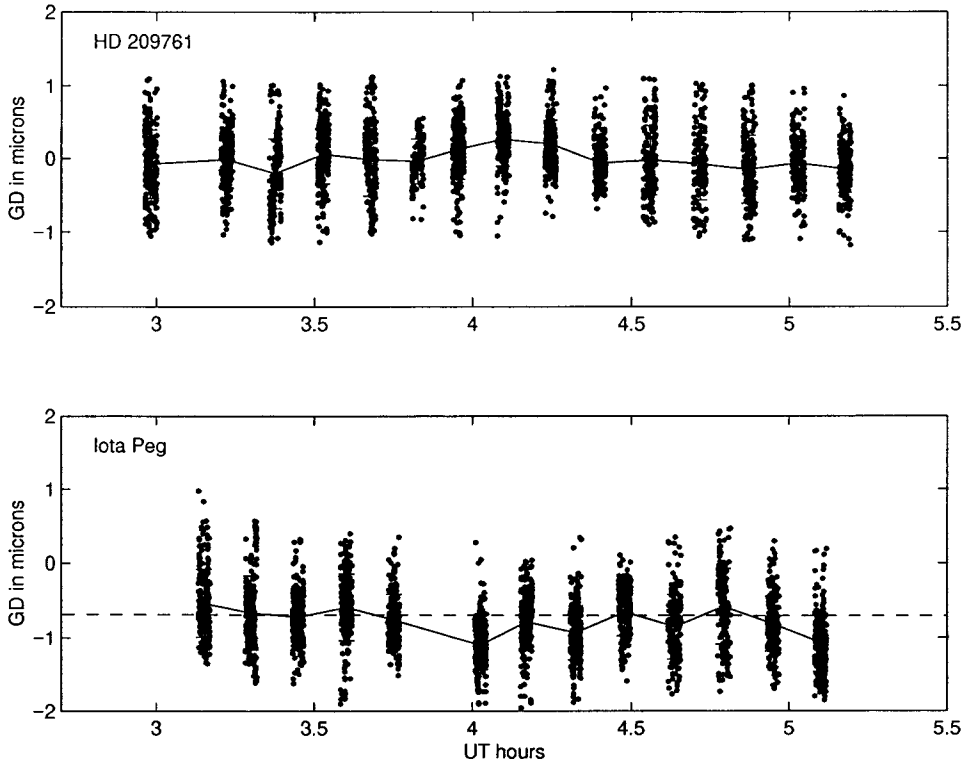

Figure 3. 99304 data. Top: HD 209761 data with sidereal fit removed (points) and 4th order polynomial fit (line). Bottom: Iota Peg (HD 210027) data with sidereal and scan averaged fit from calibrator removed (points), average of Iota Peg by scan (solid line) and predicted differential phase (dashed line). Each point represents 0.5 seconds of data.

components.

4. DIFFERENTIAL PHASE WITH THE KECK INTERFEROMETER

4.1. Candidate sources and predicted signatures

The companions to nearby stars discovered through radial velocity searches[6] are the best candidates for warm, Jupiter mass planets. As warmer planets will have a higher flux relative to the stellar flux, and therefore a larger differential phase, the planets with orbits smaller than 0.1 AU are the best targets for the Keck Interferometer (Table 1). The planet effective temperatures are calculated for an albedo of 0.25.

Observations of planet candidates found with the radial velocity technique yield the planet mass times the sine of the inclination and the orbit. Predictions for the composition and temperature of these planets come from modeling, extrapolation from our own solar system and recent spectral data from cool brown dwarfs such as Gliese 229B. To investigate the range of differential phase signatures possible from the close-in systems, we have examined models from Ref. 7–9. Models of isolated planets and brown dwarfs such as work of Ref. 10,11 are not applicable for the close-in planets due to the intense stellar radiation. A close-in planet will have a different atmospheric temperature-pressure profile as compared to an isolated planet with the same effective temperature. At the small star-planet separations considered here, reflected light from the primary will be important in some spectral regions. While reflected light will dominate thermal emission in the planet's spectrum at optical wavelengths, the reflected component is not substantial at near-infrared and longer wavelengths.[8,9]

The three modeling groups[7–9] have all produced models for 51 Peg, and we have used these models in estimating the differential phase effect. Although all groups find effective temperatures in the range 1200-1300 K, the predicted

Star Name	M*sini* M_J	Period days	Semi-major axis AU	mas	Eccentricity	T_{star} K	T_{planet} K
HD 187123	0.52	3.1	0.042	0.9	0.00	5830	1290
τ Bootis	3.64	3.3	0.042	2.7	0.00	6600	1540
HD 209458	0.69	3.5	0.045	0.001	0.0	6000	1300
HD 75289	0.42	3.5	0.046	0.016	0.053	6030	1350
51 Pegasi	0.44	4.2	0.051	3.3	0.01	5750	1230
υ Andromedae	0.63	4.6	0.053	3.9	0.03	6200	1480
HD 217107	1.28	7.1	0.07	3.5	0.14	5570	980

Table 1. Masses and orbital characteristics of the close-in candidate extrasolar planet systems. The planet temperatures are calculated for an albedo of 0.25.

infrared spectra vary from a nearly featureless, almost blackbody spectrum[7] to strong departures from blackbody due to molecular lines.[9,8] These three spectra, given in terms of planet/stellar flux ratio are shown in Figure 4. Using these spectra, the predicted differential signature in the H and K bands is roughly 0.1 milliradians. Extending the measurements to the L and M bands increases the signature to ~0.3 milliradians due to the higher planet/stellar flux ratio at these wavelengths.

4.2. Observations and systematics

To measure the differential phase at the levels predicted above, minimization of the atmospheric and instrumental terms is essential. As discussed in section 3.2, water vapor fluctuations are the dominate contribution to the infrared dispersion. However, the dispersion changes due to temperature fluctuations are larger than the predicted differential phase signature for close-in extrasolar planets and must also be removed. Contributions from instrument systematics are important at the level of tenths of milliradians. In particular, the delay line stroke, fringe wavelength and beam walk must be well calibrated.

ACKNOWLEDGMENTS

This work was performed at the Infrared Processing and Analysis Center, Caltech and the Jet Propulsion Laboratory. PTI is funded by NASA contracts with the Jet Propulsion Laboratory. Observations at PTI are possible through the efforts of the PTI Collaboration (`http://huey.jpl.nasa.gov/palomar/ptimembers.html`).

REFERENCES

1. M. Colavita et al, "The Palomar Testbed Interferometer," *Ap. J.* **510**, pp. 505–521, 1999.
2. M. Colavita, "Fringe visibility estimators for the Palomar Testbed Interferometer," *PASP* **111**, pp. 111–117, 1999.
3. A. Boden, C. Koresko, G. van Belle, M. Colavita, P. Dumont, J. Gubler, S. Kulkarni, B. Lane, D. Mobley, M. Shao, J. Wallace, and G. Henry, "The visual orbit of iota Pegasi," *Ap. J.* **515**, pp. 356–364, 1999.
4. J. Owens, "Optical refractive index of air: dependence on pressure, temperature and composition," *Appl. Opt.* **6**, pp. 51–59, 1967.
5. R. Hill and R. Lawrence, "Refractive index of water vapor in infrared windows," *Infrared Phys.* **26**, pp. 371–376, 1986.
6. G. Marcy and R. P. Butler, "Detection of extrasolar giant planets," *ARAA* **36**, pp. 57–97, 1998.
7. F. Allard, "Models, atmospheres, and spectra of brown dwarfs to giant planets," in *From giant planets to cool stars*, M. Marley, ed., 1999.
8. C. Goukenleuque, "Radiative equilibrium model of 51 Peg," in *From giant planets to cool stars*, M. Marley, ed., 1999.
9. S. Seager and D. Sasselov, "Extrasolar giant planets under strong stellar irradiation," *Ap. J. Letters* **502**, pp. 157–160, 1998.

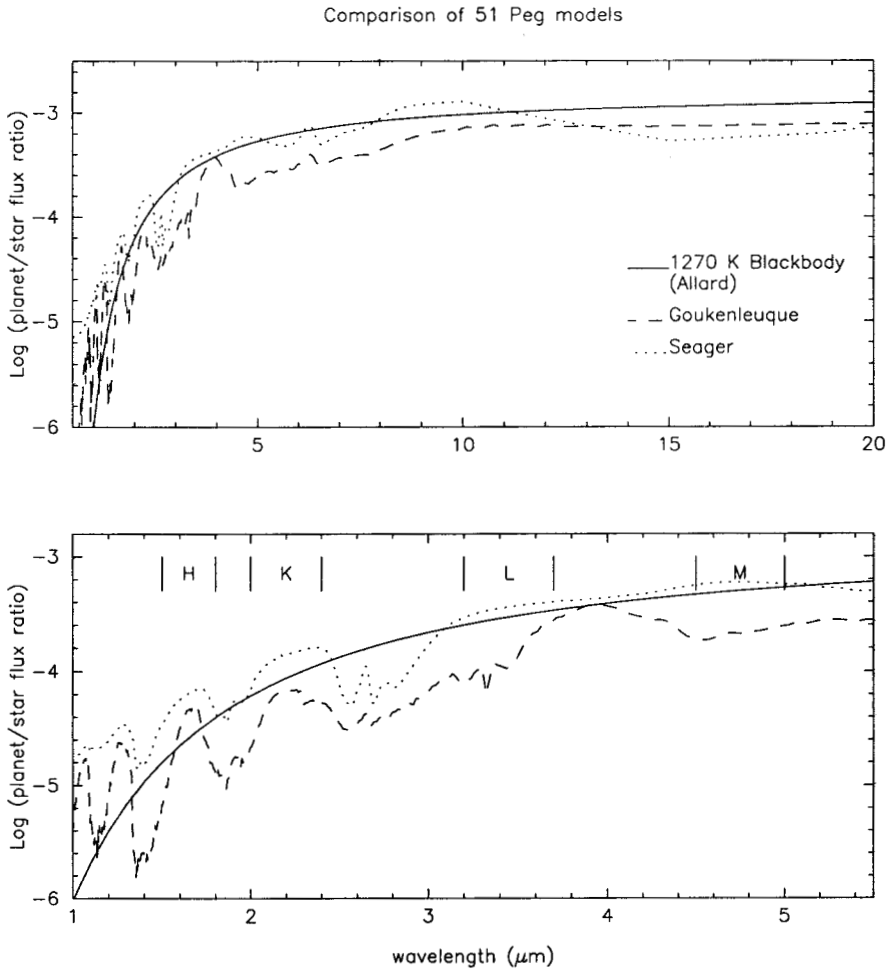

Figure 4. Ratio of planet to stellar flux for three models of the 51 Peg system. The spectra are taken from Ref. 7-9.

10. F. Allard, P. Hauschildt, I. Baraffe, and G. Chabrier, "Synthetic spectra and mass determination of the brown dwarf Gliese 229B," *Ap. J. Letters* **465**, pp. 123–127, 1996.
11. A. Burrows, M. Marley, W. Hubbard, J. Lunine, T. Guillot, D. Saumon, R. Freedman, D. Sudarsky, and C. Sharp, "A nongray theory of extrasolar giant planets and brown dwarfs," *Ap. J.* **491**, pp. 856–875, 1997.